01 Jan 2014

Synthesis, Optical Properties and Photovoltaic Applications of Hybrid Rod-coil Diblock Copolymers with Coordinatively Attached CdSe Nanocrystals

Shaohua Li

Yong Li

Clarissa A. Wisner

Lu Jin

et. al. For a complete list of authors, see https://scholarsmine.mst.edu/chem_facwork/2123

Recommended Citation

S. Li et al., "Synthesis, Optical Properties and Photovoltaic Applications of Hybrid Rod-coil Diblock Copolymers with Coordinatively Attached CdSe Nanocrystals," *RSC Advances*, vol. 4, no. 68, pp. 35823-35832, Royal Society of Chemistry, Jan 2014.
The definitive version is available at https://doi.org/10.1039/c4ra04347b

RSC Advances

PAPER

View Article Online
View Journal | View Issue

Cite this: *RSC Adv.*, 2014, **4**, 35823

Synthesis, optical properties and photovoltaic applications of hybrid rod–coil diblock copolymers with coordinatively attached CdSe nanocrystals†

Shaohua Li,‡[a] Yong Li,‡[a] Clarissa A. Wisner,[b] Lu Jin,[a] Nicholas Leventis[b] and Zhonghua Peng*[a]

The performance of hybrid solar cells based on conjugated polymers and nanostructured inorganic semiconductors is often limited by the poor interfacial interaction and the lack of controlled phase separation. Improvements are being made by building intimate contact between the two components through coordinative linkages. In this contribution, three rod–coil diblock copolymers (DCPs) of the modified poly(3-hexylthiophene)-polystyrene (P3HT-PS) type with different phosphorus-containing functional groups for binding to inorganic nanoparticles are reported. Their corresponding P3HT-PS-CdSe hybrid DCPs (HDCPs) were prepared by ligand-exchange with chemically prepared CdSe nanocrystals. The three DCPs have different size disparity between the rod and coil blocks, where the dominant block dictates their solid state aggregation behavior. As a result, the three DCPs show very different fluorescence properties in the solid state. After binding with CdSe nanocrystals, nanocrystal association appears to dominate the solid state aggregation in all three HDCPs, making them exhibit comparable solid state optical properties. Solar cell devices of HDCPs showed high open circuit voltages of 1.13–1.40 V and improved power conversion efficiencies (PCEs) over devices fabricated from the corresponding DCPs without CdSe attachment. It is believed that the improvement of the PCE is brought about by intimate contact between the P3HT and the CdSe components, which enhances the initial charge separation from P3HT to the CdSe nanocrystals. The device performance is however hampered by the low nanoparticle loading and the short P3HT block length, which are being addressed.

Received 9th May 2014
Accepted 8th August 2014

DOI: 10.1039/c4ra04347b

www.rsc.org/advances

1 Introduction

Organic–inorganic hybrid solar cells (HSCs) have drawn increasing attention in recent years as a promising photovoltaic technology.[1–5] HSCs composed of either bulk[6–8] or ordered[9–12] heterojunctions of conjugated polymers and inorganic semiconductor nanostructures have been demonstrated and their device efficiencies have been steadily climbing.[5,13] Poly(3-hexylthiophene-2,5-diyl) (P3HT), as a benchmark photovoltaic material, is one of the most extensively utilized conjugated polymers in HSCs.[5,6] Composites based on P3HT and inorganic semiconductors of different compositions (such as Si,[14] CdS,[15,16] CdSe,[9,17,18] CdTe,[19,20] $CuInSe_2$,[21] PbS,[22] TiO_2,[23,24] and ZnO,[25,26] *etc.*) and of different nanostructures (nanoparticles,[19] nanocrystals (NCs),[14] quantum dots, nanowires,[16] nanorods,[15,17,20] nanoporous structures,[27] *etc.*) have been studied in solar cell devices. In these HSCs, P3HT often plays the roles of photosensitizer, excitonic electron donor and hole transporter, while the inorganic components serve as electron acceptors and electron transporters. It is envisioned that the high charge carrier mobility of inorganic semiconductors may help lead to significantly enhanced photoinduced charge separation efficiencies due to fast electron dissipation through the semiconductor network.[5]

HSCs may be fabricated by using simple physical mixtures of P3HT and inorganic semiconductors. These composites, however, without strong chemical interactions between the organic and inorganic components, often exhibit inefficient interfacial charge separation.[28] In addition, because of the drastic structural and property differences between those two components, macroscopic phase separation is almost inevitable, which eventually limits the performance and long-term stability of the resulting devices.[29] To improve the compatibility and to ensure intimate contact between the two components as well as the structural stability of the blend films, researchers have developed some viable approaches such as

[a]*Department of Chemistry, University of Missouri-Kansas City, Kansas City, Missouri 64110, USA. E-mail: pengz@umkc.edu; Fax: +1-816-235-2290; Tel: +1-816-235-2288*
[b]*Department of Chemistry, Missouri University of Science and Technology, Rolla, Missouri 65409, USA*

† Electronic supplementary information (ESI) available: The synthesis, absorption and fluorescence spectra of HDA/TOPO-capped CdSe NCs, the MALDI-TOF MS results of the vinyl-terminated P3HT and the **P3HT-MI**, FT-IR of **P3HT-PS-2** and **P3HT-PS-CdSe-2**, EDX analysis of HDCPs, the calculation of the weight ratio of the hybrids, TGA figures of DCPs and HDCPs, and the *J–V* curves of the solar cells of HDCPs are included. See DOI: 10.1039/c4ra04347b

‡ These authors contributed equally to this work.

surface modification on the inorganic component or the attachment of inorganic-binding ligands to the organic component.[24,30–33] Typically, a binding ligand is attached to the end of a conjugated oligomer or polymer which is then grafted to the surface of an inorganic nanostructure to form the organic–inorganic hybrids.[32,33] Improved compatibility between and enhanced charge separation across the organic and inorganic components have been demonstrated. Herein, we report the detailed synthesis, optical property studies and photovoltaic performance evaluations of three hybrid rod–coil diblock copolymers of modified P3HT-polystyrene (P3HT-PS) with coordinatively attached CdSe nanocrystals in the coil block. Rod–coil diblock copolymers (DCPs) are an important class of block polymers with potentially hierarchical ordered structures at multiple length scale.[34–36] The rigid rod block, mostly an extended π-conjugated system, is usually a liquid-crystal-forming mesogen which plays an important role during microphase separation. Having semiconducting nanoparticles attached to the coil block helps preserve π-stacking of the rod block while at the same time promotes microphase separation due to the extreme contrast in architecture between the two blocks. Such hybrid diblock copolymers are thus potentially attractive systems for HSCs.

Fig. 1 shows the structures of the reported hybrid systems. The rod block is P3HT while the coil block is PS which is chemically-modified with phosphorus-containing functional groups as pendants. It is envisioned that having multiple binding ligands in the PS block helps create a tight and strong binding between the DCP and the nanoparticles,[37,38] which can be conducive to efficient photoinduced charge transfer. Solar cells fabricated from these hybrids indeed showed improved performances over devices fabricated from the corresponding DCPs without CdSe coordination and devices of covalently bonded donor–acceptor DCPs.

2 Experimental

2.1 Materials and characterization

All chemicals were purchased from Aldrich or Acros and were used without further purification unless otherwise noted. ^{1}H, ^{13}C and ^{31}P NMR spectra were recorded in $CDCl_3$ on a Varian INOVA 400 MHz FTNMR spectrometer. All samples were referenced to the deuterated solvent for the ^{1}H and ^{13}C NMR measurements, while triphenylphosphine (TPP) was applied as an internal standard for the ^{31}P NMR measurements. Mass measurements were carried out on a Voyager DE Pro (Perceptive Biosystems/ABI) MALDI-TOF mass spectrometer with dithranol (1,8-dihydroxyanthrone) was used as the matrix. Gel permeation chromatography (GPC) measurements were performed on a Tosoh Ecosec HLC-8320GPC system equipped with triple detectors (a differential refractometer, a light scattering detector, and a UV detector) and a styragel column. THF was used as the mobile phase. The instrument was calibrated by the use of five polystyrene standards ranging from 8000 to 90 000 in number-average molecular weights. FT-IR spectra were recorded on a Shimadzu IRAffinity-1 FTIR spectrophotometer. Transmission electron microscopy (TEM) images were taken using a FEI Tecnai F20 200 kV super twin lens TEM in standard mode. Thermal gravimetric analyses were performed on Shimadzu TGA-50. UV/Vis absorption spectra were collected on a Hewlett-Packard 8452A diode array spectrophotometer. Fluorescence spectra were measured with a Shimadzu RF-5301 PC spectrofluorophotometer. Fluorescence quantum yields for solutions were calculated with quinine sulfate in 1 N H_2SO_4 ($\varphi_{fl} \approx 0.58$) as the standard. Cyclic voltammetry studies were performed with a BAS Epsilon EC electrochemical station, using a Pt working electrode of 1.6 mm in diameter, a silver wire as the reference electrode and a Pt wire as the counter electrode under argon protection. A 0.1 M tetra-*n*-butylammonium hexafluorophosphate solution in acetonitrile was used as supporting electrolyte. Calibration of the potential was carried out by a ferrocene/ferrocenium (Fc/Fc^+) redox couple whose absolute energy was assigned as −4.80 eV *vs.* vacuum. The highest occupied molecular orbital (HOMO) and the lowest unoccupied molecular orbital (LUMO) energy levels were calculated by HOMO $= -(E_{ox}^{onset} + 4.80)$ (eV) and LUMO $= -(E_{red}^{onset} + 4.80)$ (eV), respectively.

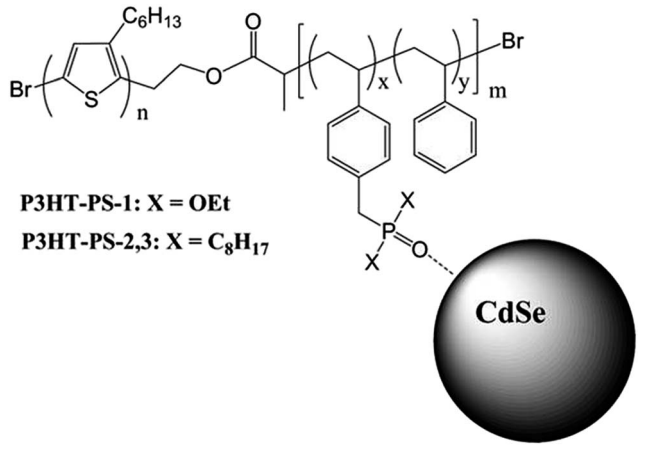

Fig. 1 Hybrids of P3HT-polystyrene diblock copolymers with CdSe nanoparticles.

2.2 Synthesis of modified P3HT-PS DCPs

Diethyl (4-vinylbenzyl)phosphonate (M1).[39] *p*-Vinylbenzyl chloride (2.15 g, 14.1 mmol) was first stirred with NaI (10.5 g, 70.4 mmol) in acetone solution (40 mL) overnight. Ether (30 mL) was added to the reaction mixture, which was then washed three times with deionized water (100 mL). The formed vinylbenzyl iodide was collected by removing the organic solvents under vacuum, which was then stirred with triethylphosphite (2.34 g, 14.1 mmol) at room temperature for 12 h. The side product (iodoethane) was removed by rotary evaporation, and column chromatography purification of the product on silica gel with dichloromethane as the eluent afforded diethyl(4-vinylbenzyl) phosphonate as pale yellow liquid (3.34 g, 93% yield). ^{1}H NMR (400 MHz, $CDCl_3$): δ/ppm = 7.36 (d, J = 8.0 Hz, 2H), 7.25 (d, J = 10.4 Hz, 2H), 6.69 (dd, J = 10.8 Hz, 18.0 Hz, 1H), 5.73 (d, J = 17.6 Hz, 1H), 5.22 (d, J = 17.6 Hz, 1H), 4.11–3.92 (m, 4H), 3.14 (d, J = 21.6 Hz, 2H), 1.23 (t, J = 7.2 Hz, 6H); ^{13}C NMR (400 MHz, $CDCl_3$): δ/ppm = 135.7, 135.6, 130.8, 129.2, 125.8, 113.1, 61.4, 33.5, 32.2, 15.8; ^{31}P NMR (400 MHz, $CDCl_3$): δ/ppm = 21.2.

Dioctyl (4-vinylbenzyl)phosphine oxide (M2). The mixture containing *p*-vinylbenzyl chloride (0.152 g, 1 mmol), dioctyl phosphine oxide (0.220 g, 0.8 mmol), $(TBA)_2SO_4$ (29 mg), toluene (3 mL) and 30% NaOH (1.2 mL) was stirred for 24 h. The organic phase was washed with water, and the product was precipitated by adding hexane. Recrystallization of the precipitates from hexane afforded the title product as white solids (0.312 g, 91% yield). ^{1}H NMR (400 MHz, $CDCl_3$): δ/ppm = 7.36 (d, J = 8.0 Hz, 2H), 7.18 (d, J = 10.4 Hz, 2H), 6.68 (dd, J = 10.8 Hz, 17.6 Hz, 1H), 5.72 (d, J = 17.6 Hz, 1H), 5.23 (d, J = 10.8 Hz,1H), 3.10 (d, J = 14.4 Hz, 2H), 1.6–1.5 (m, 8H), 1.4–1.2 (m, 20H), 0.87 (t, J = 6.8 Hz, 6H); ^{13}C NMR (400 MHz, $CDCl_3$): δ/ppm = 136.2, 131.8, 129.6, 129.0, 126.6, 113.4, 35.7, 32.2, 30.9, 28.8, 27.3, 26.7, 22.5, 21.4, 14.0; ^{31}P NMR (400 MHz, $CDCl_3$): δ/ppm = 47.0.

Poly(3-hexylthiophene) macroinitiator (P3HT-MI).[40] A sample of 2-bromopropionyl bromide (1.5 mL, 12 mmol) was added dropwise into a solution containing P3HT-OH (0.49 g, 0.02 mmol), triethylamine (2 mL, 14.7 mmol) and anhydrous THF (20 mL) at room temperature under N_2. After being stirred at 40 °C for 24 h, the solution was poured into methanol. The polymer precipitates were collected by filtration and purified by Soxhlet extraction with methanol and hexane. Yield: 96%. ^{1}H NMR (400 MHz, $CDCl_3$): δ/ppm = 6.96 (br), 4.35 (m), 3.11 (t, J = 7.2 Hz), 2.78 (br), 1.83 (d, J = 6.8 Hz), 1.68 (br), 1.5–1.3 (br), 0.89 (s).

P3HT-PS-1,2,3. All three DCPs were prepared by the atom transfer radical polymerization (ATRP).[41,42] In a typical polymerization process, CuBr, *N*,*N*,*N*′,*N*″,*N*″-pentamethyldiethylenetriamine (PMDETA, ligand), and styrene (M) together with the modified styrene monomer (M1 or M2) were added to dry *p*-xylene. The reaction mixture was degassed by three freeze–pump–thaw cycles, and then filled with N_2 gas. A degassed solution of **P3HT-MI** in *p*-xylene (1 mL) was then added, and the reaction mixture was stirred at 110 °C for 24 h under N_2 atmosphere. For **P3HT-PS-1**, styrene and M1 were used as monomers with a molar ratio of 1 : 1. For **P3HT-PS-2**, and **P3HT-PS-3**, styrene and M2 were used as monomers with a molar ratio of 1 : 1 and 4 : 1, respectively. The mole ratio of $[M]_{total}$: [**P3HT-MI**] : [CuBr] : [PMDETA] was set to be 100 : 1 : 1 : 6 for **P3HT-PS-1** and **P3HT-PS-2**, while 250 : 1 : 20 : 120 for **P3HT-PS-3**. After cooled to room temperature, a minute amount of THF was added to the dark-red solution. The solution was then passed through a short neutral Al_2O_3 column to remove the copper catalyst. The eluent was poured into methanol and the resulting precipitates were collected by centrifugation. The collected polymers were redissolved in THF and reprecipitated from methanol to give the corresponding diblock copolymers.

P3HT-PS-1 (23%). ^{1}H NMR (400 MHz, $CDCl_3$): δ/ppm = 7.02 (br), 6.97 (s), 6.50 (br), 3.96 (br), 3.04 (br), 2.79 (br), 1.84 (br), 1.69 (br), 1.4–1.1 (br), 0.90 (br). ^{31}P NMR (400 MHz, $CDCl_3$): δ/ppm = 22.1.

P3HT-PS-2 (17%). ^{1}H NMR (400 MHz, $CDCl_3$): δ/ppm = 7.02 (br), 6.96 (s), 6.43 (br), 3.10 (br), 2.78–2.60 (br), 2.0–1.1 (br), 0.88 (br). ^{31}P NMR (400 MHz, $CDCl_3$): δ/ppm = 48.1.

P3HT-PS-3 (22%). ^{1}H NMR (400 MHz, $CDCl_3$): δ/ppm = 7.05 (br), 6.97 (s), 6.52 (br), 3.09 (br), 2.79 (br), 2.3–1.2 (br), 0.89 (br). ^{31}P NMR (400 MHz, $CDCl_3$): δ/ppm = 46.0.

P3HT-PS-n-CdSe. Detailed preparation of HDA/TOPO-capped CdSe nanocrystals was described in the ESI.† The as-prepared CdSe nanocrystals (100 mg) were stirred at 90 °C in pyridine (10 mL) for 12 h. After cooled to room temperature, hexane was added to the solution and pyridine-capped CdSe nanocrystals were precipitated and collected by centrifuge. This process was repeated for two additional times. The resulting pyridine-capped CdSe nanocrystals were collected and dried with a stream of nitrogen gas. Pyridine-capped CdSe nanocrystals (10 mg) were added to a solution of **P3HT-PS-n** (20 mg) in THF (5 mL), and the suspension was subjected to ultrasonication for 3 h. The mixture was cooled to room temperature and then passed through a 0.45 μm filter, where the undissolved pyridine-capped CdSe nanocrystals were removed. Acetone was added to the clear filtrate solution and the precipitated **P3HT-PS-n-CdSe** nanocomposites were collected by centrifuge. The precipitated nanocomposites were further washed with methanol and acetone for a few times.

2.3 Photovoltaic devices fabrication and characterization

Indium tin oxide (ITO) coated glass (Delta Technologies; sheet resistance, 8–12 Ω per square) was used as substrates. Under the protection of Magic tape, the ITO side of each substrate was patterned by etching with aqua regia vapor. The patterned ITO glass substrates were cleaned in an ultrasonic bath sequentially by hot detergent, water, deionized water, toluene, acetone, and isopropyl alcohol, and then dried by compressed air. Cleaned ITO substrates were treated with UV ozone for 45 min before use. Highly conductive poly(3,4-ethylenedioxythiophene):poly(styrenesulfonate) (PEDOT:PSS; Heraeus Precious Metals; Clevios P VP AI4083) thin layer was spin-coated (4000 RPM, 30 s) onto the ITO substrates from an aqueous solution. The PEDOT:PSS thin films were dried at 120 °C for 45 min on hotplate in air. The **P3HT-PS-CdSe-1**, **P3HT-PS-CdSe-2**, and **P3HT-PS-CdSe-3** solutions were prepared in chloroform with concentration of 5 mg mL^{-1}. The above solutions were passed through a 0.45 μm filter and spin-coated on top of the PEDOT:PSS layer at 400 RPM for 30 s. The devices were transferred into a glove box and thermally annealed there at 120 °C for 10 min in dark. Subsequently, electrodes composed of 45 nm thick Ca and 100 nm thick Al were deposited on top in sequence by thermal evaporation under high vacuum ($<2 \times 10^{-6}$ mb) through a shadow mask. The active area of 0.14 cm^2 of the devices was defined by the overlapped area of the ITO and the deposited Ca/Al electrodes. Current–voltage characteristics of the solar cells were measured using a Keithley 2400 Source Meter. Incident photon to current conversion efficiency (IPCE) spectra were recorded using a Newport QE-PV-SI QE/IPCE measurement kit. The thickness of the thin films was measured with a Tencor Alphastep 200 automatic step profiler.

3 Results and discussion

Scheme 1 shows the synthesis of the three hybrid DCPs. A P3HT rod block end-functionalized with α-bromopropanoate (**P3HT-MI**),

was synthesized following literature procedures[40] and was used as a macroinitiator to grow the coil block using atom-transfer radical polymerization (ATRP).[41,42] All three DCPs have the same P3HT block length with an average molecular weight of 2338 (average number of repeating unit 14) and a polydispersity of 1.03, measured by MALDI-TOF mass spectrometry. The P3HT with shorter chain length was selected here as it has a higher solubility in THF to ensure a better functionalization with the end group and a narrow molecular weight distribution. To realize a coil block which can bind to CdSe nanoparticles, two styrene derivatives, one functionalized with a phosphonate group (M1) and the other with a phosphine oxide (M2), both of which are well known ligands for CdSe binding, were synthesized as monomers for ATRP. M1 or M2 was copolymerized with styrene in a 1 : 1 or 1 : 4 monomer ratio to ensure the incorporation of sufficient binding ligands in the coil block but without steric congestion. Using M1 and M2 respectively as the functionalized monomer, **P3HT-PS-1** and **P3HT-PS-2** were synthesized under identical ATRP conditions, leading to coil blocks with comparable sizes. **P3HT-PS-3**, on the other hand, was synthesized using a much higher monomer-to-initiator ratio, resulting in a DCP with a much longer coil block. All three DCPs show excellent solubility in chloroform and THF, and are moderately soluble in acetone.

Fig. 2 shows the ^{1}H NMR spectra of the three DCPs. While the signals are broad and most are significantly overlapped, one can still identify certain signals which are characteristic to each repeating unit. For example, signals marked as 1, 2 and 3 in Fig. 2 can be attributed to the 3-hexylthiophene unit. The phosphonate or phosphine oxide-functionalized styrene units give distinct signals marked as a, b, c, d and e. The phenyl protons (α, β) of styrene are overlapped with those of M1 or M2 (a & b). Based on the integration of the characteristic signals, one can calculate the diblock copolymer compositions. For

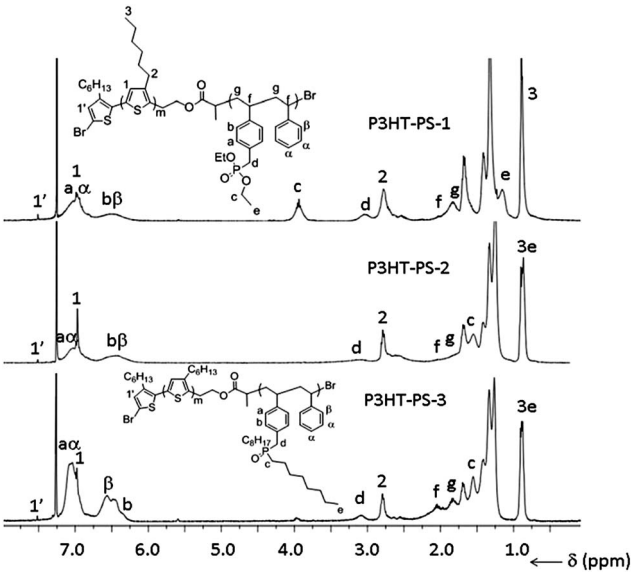

Fig. 2 ^{1}H NMR spectra of **P3HT-PS-1,2,3** in $CDCl_3$.

P3HT-PS-1, using the integration ratio of well resolved signals 3 and c (4 : 1), one can calculate the average number of M1 unit in the diblock copolymer to be 3 (the average number of P3HT repeating unit is 14 based on MALDI-TOF measurements). With P3HT and M1 compositions in the DCP known and using the integration of the aromatic signals (either a/1/α or b/β or both), one can calculate the number of styrene units in the DCP to be 5, giving **P3HT-PS-1** an average molecular weight of 3640. For the other two DCPs, well-resolved signal 2 was used as the reference for the P3HT block. Based on the integration of signals 3/e and 2, one can calculate the number of protons corresponding to proton e, and thus the number of repeating

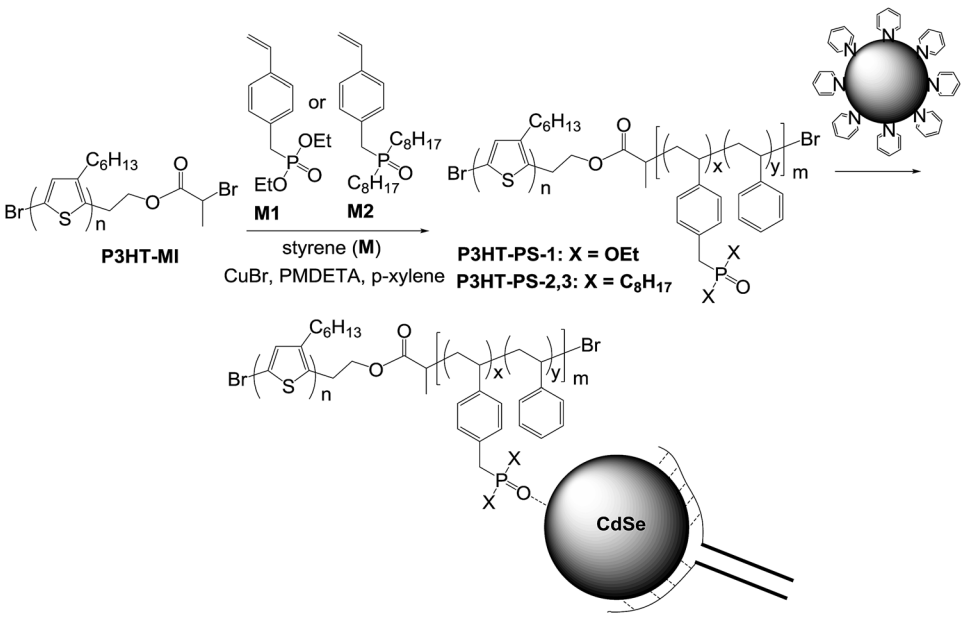

Scheme 1 Synthesis of P3HT-PS DCPs and ligand exchange with pyridine-capped CdSe nanocrystals.

unit M2. Once the P3HT and M2 compositions in the DCP are known, the integration ratio of the aromatic signals *versus* that of 2 can be used to calculate the number of styrene repeating unit. Following these procedures, the number of M2 and styrene repeating units in **P3HT-PS-2** and **P3HT-PS-3** are found to be 5 and 7, 12 and 51, respectively, from which their number-average molecular weights are calculated to be 5038 and 12 355, respectively. These numbers are rather consistent with the molecular weights measured by Gel Permeation Chromatography (GPC), which gave M_ns of 4975, 5499, and 14 822 for **P3HT-PS-1**, **P3HT-PS-2** and **P3HT-PS-3**, respectively. The coil block compositions in all three DCPs reasonably match the monomer loading ratios with styrene only in slight excess, indicating that M1 and M2 have similar reactivity to the styrene monomer.

CdSe nanocrystals with average sizes around 5 nm were synthesized using the well demonstrated hot-injection method.[43] The original hexadecylamine (HAD) and trioctylphosphine oxide (TOPO) capping ligands on the CdSe nanocrystals were first replaced with pyridine, which was then exchanged with the ligands on the DCPs, as shown in Scheme 1. Compared to the direct growth of nanocrystals in the DCP matrix, this process is advantageous since nanocrystals are synthesized separately, allowing much better control in their size and size distribution. The ligand exchange was carried out in THF where the pyridine-capped CdSe nanocrystals are not soluble. Excess non-DCP bound nanocrystals were got rid of by filtration. The CdSe-coordinated HDCPs were isolated by precipitating from acetone where any DCPs without CdSe binding remain soluble. The as-prepared hybrids are soluble in chloroform and THF.

The formation of DCP–CdSe hybrids was confirmed by FT-IR, TEM and SEM-EDX analysis (see Fig. S7–S9 in ESI†). Fig. 3 shows the FT-IR spectra of **P3HT-PS-1**,**3** before and after CdSe coordination. For all DCPs, the IR absorption at 2960–2860 cm^{-1} (C–H stretching) and 1730–1600 cm^{-1} (aromatic C=C stretching) can be clearly observed. The characteristic P=O stretching band appears at around 1250–1260 cm^{-1}, indicating the existence of phosphonate or phosphine oxide groups. After CdSe coordination, those P=O stretching bands shift to lower wavenumbers, indicating O–Cd binding which weakens the P=O bond.[44]

High-resolution TEM images of the three DCP–CdSe hybrids were collected (Fig. 4). CdSe nanocrystals with distinct crystalline lattice fringe can be clearly observed in all three composite samples, and the average size of nanocrystals is around 5 nm. The lattice fringe spacing of the CdSe NCs is measured to be 0.334 nm and is consistent with the lattice spacing of CdSe NCs with the Wurtzite structure.[45] The inset in Fig. 4d shows the fast Fourier transformation (FFT) pattern of **P3HT-PS-CdSe-3** hybrids, from which the crystallinity of the CdSe nanocrystals was confirmed. As can be seen from all images, the CdSe nanocrystals are uniformly distributed among all DCP substrates although some aggregation is noted. The aggregation may be due to the binding of one DCP to more than one nanocrystal since each coil block has multiple binding ligands.

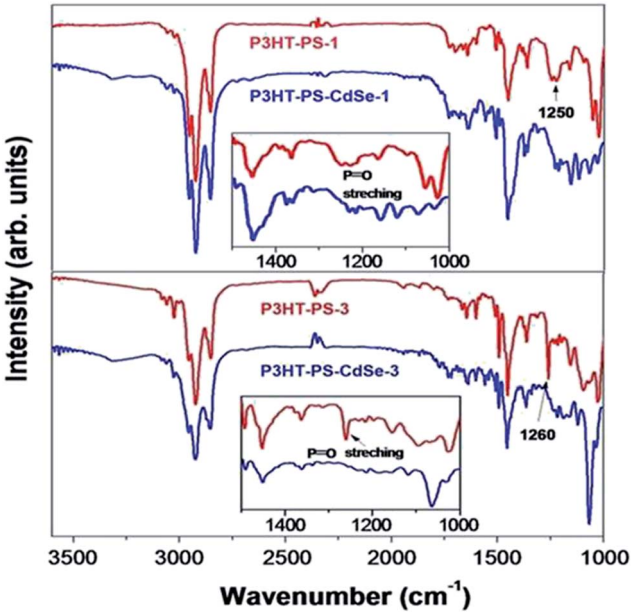

Fig. 3 FT-IR spectra of **P3HT-PS-1,3** and **P3HT-PS-CdSe-1,3**.

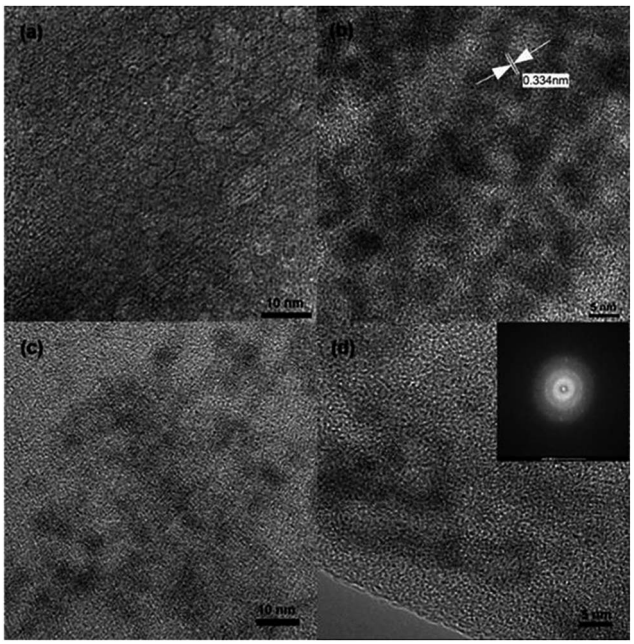

Fig. 4 HRTEM images of (a) **P3HT-PS-CdSe-1**, (b) **P3HT-PS-CdSe-2**, (c) and (d) **P3HT-PS-CdSe-3**. The inset in (d) displays the fast Fourier transformation (FFT) pattern of the nanocrystals in **P3HT-PS-CdSe-3**.

The UV/Vis absorption spectra of DCPs before and after CdSe coordination are shown in Fig. 5. The spectra are dominated by the absorption of the P3HT block with an absorption maximum around 438 nm. After CdSe coordination, this band is slightly red-shifted, and a well separated weak absorption band at 570–580 nm is observed for all three hybrids as shown clearly in the inset of Fig. 5. This absorption is attributed to CdSe NCs. It is noted that the absorption maxima of the CdSe NCs in the hybrid DCPs are slightly red-shifted compared to that of the original

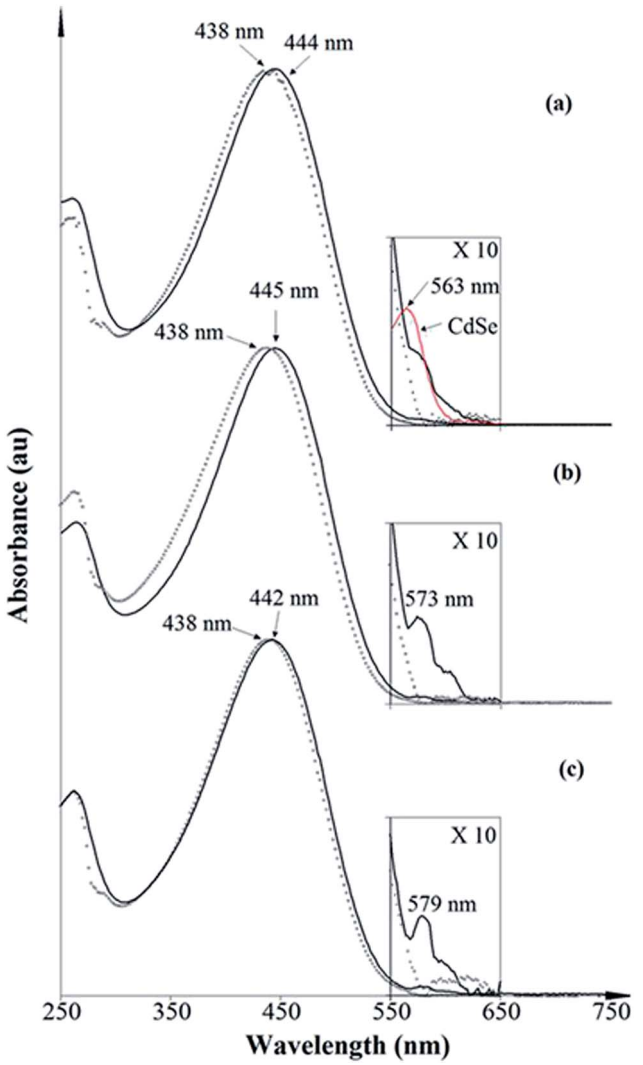

Fig. 5 UV/Vis absorption spectra of P3HT-PS-1 (a), 2 (b) and 3 (c) before (dotted) and after (solid) CdSe coordination.

TOPO-capped CdSe NCs (563 nm). The 10 to 15 nm redshift may be due to the change in surface ligands (for **P3HT-PS-1**) or ligand densities (for **P3HT-PS-2** and **P3HT-PS-3**). Note that the extent of redshift increases from **P3HT-PS-1**, to **P3HT-PS-2** and to **P3HT-PS-3**. Using a **P3HT-MI** solution and a TOPO-capped CdSe NC solution with known concentrations as standards and assuming that the total weight of surface ligands are negligible compared to the weight of the core NCs, one can calculate the DCP–CdSe weight ratio in the hybrids using the absorbance at 444 nm and the maximum absorption wavelength in the 560–580 nm range. Using this method, the CdSe–DCP weight ratios are estimated to be 1 : 12, 1 : 8, and 1 : 11 for **P3HT-PS-1,2,3** respectively (see ESI† for the detailed calculation). While this estimate is very rough, it nonetheless indicates that the nanocrystal contents in all three hybrids are rather low.

The amount of NCs in the HDCPs was also estimated by the thermogravimetric analysis (TGA) (see Fig. S10 in ESI†). All DCPs and HDCPs were heated, under N_2 protection, from room temperature to 600 °C at a rate of 10 °C min^{-1}. For all polymers, weight loss occurred in the temperature range of 200–480 °C. No or negligible further weight loss was observed up to 600 °C. At 600 °C, the remaining weight percentage is 42, 38 and 36%, for **P3HT-PS-1**, **P3HT-PS-2**, **P3HT-PS-3**, respectively. Their corresponding HDCPs at 600 °C have higher remaining weights of 62, 63, and 41%. Assuming CdSe is not losing weight in the heating process, and the difference in remaining weight percentage between the HDCPs and their corresponding DCPs at 600 °C is due to the coordinated CdSe NCs, one can calculate the weight percentage of the NCs in the original HDCPs to be 34, 40, and 8%, respectively. While these values are higher than those estimated based on UV/Vis absorption spectra, both techniques indicate that **P3HT-PS-CdSe-2** has the highest CdSe NC loading.

The absorption spectra of the DCP films before and after CdSe coordination have also been studied. As shown in Fig. 6, all DCP films show a broad absorption peak at 483–492 nm, over 40 nm red-shifted compared to that of their solution spectra. Such red shifts are common for P3HT-containing DCPs due to the P3HT inter-chain π-stacking in the thin solid films.[46] It is noted that both the maximum absorption wavelength and the absorption band edge of **P3HT-PS-3** film are clearly shorter than those of the other two DCPs, indicating that the P3HT

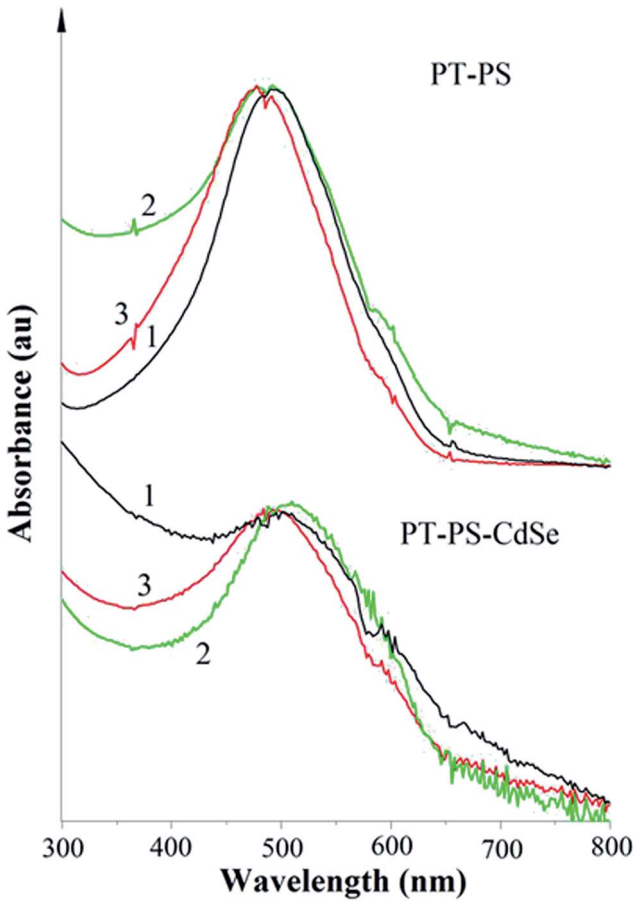

Fig. 6 UV/Vis absorption spectra of thin films of DCPs before and after CdSe coordination.

π-stacking in **P3HT-PS-3** is not as strong as in the other two DCPs. In **P3HT-PS-1** and **P3HT-PS-2**, the P3HT block is longer than the PS block and likely dictates the diblock copolymer aggregation. In **P3HT-PS-3**, however, the PS block is about 4 times as long as the P3HT block, and thus likely dominates the self-assemble of the diblock copolymer. In other words, the arrangement of P3HT blocks in **P3HT-PS-3** is dictated not so much by their own π–π stacking but by PS blocks, making P3HT stacking not as effective. After the coordination of CdSe NCs, the absorption of all hybrid films further red-shifted to 496–511 nm. The maximum absorption wavelength of **P3HT-PS-CdSe-3** is again shorter than those of the other two HDCPs.

The fluorescence emission spectra of DCPs and HDCPs in chloroform solutions and as solid films have been studied. As shown in Fig. 7, when excited at 440 nm, all DCP and HDCP solutions show nearly identical fluorescence emission spectra and comparable fluorescence quantum yields (~0.065). The typical narrow emission of CdSe NCs (see Fig. S4 in ESI†) was not discernable in the emission spectra of the hybrids, most likely overshadowed by the broad emission of P3HT segments. The lack of fluorescence quenching indicates that the energy/electron transfer from the photoexcited P3HT chromophores to the CdSe NCs is inefficient in dilute solutions. In solid state, the three DCPs show very different emission spectra. While films of **P3HT-PS-1** and **P3HT-PS-2** both gave an emission maxima at 636 nm, the maximum emission wavelength of **P3HT-PS-3** film is only 576 nm, less than 10 nm red-shifted over its solution emission spectrum. As explained earlier, the π-stacking of P3HT in **P3HT-PS-3** is not the driving force for the DCP self-assembly but rather the interaction among the much longer PS blocks, which accounts for its much less red-shifted emissions. The binding of CdSe NCs to the PS block resulted in starkly different changes in their films' fluorescence emissions. While the binding of CdSe NCs leads to negligible change in the film emission spectrum of **P3HT-PS-2**, the emission spectra of **P3HT-PS-1** are blue shifted by 21 nm while those of **P3HT-PS-3** are red-shifted by 34 nm after CdSe NCs were coordinated. It is interesting to note that the relative sizes of the P3HT block and the PS block change from P3HT dominant (**P3HT-PS-1**) to comparable (**P3HT-PS-2**) to PS dominant (**P3HT-PS-3**). The different size disparity in the three DCPs likely gives rise to their different emission changes in responding to CdSe NC binding. It is noted that the film emission spectra of the three HDCPs do not differ as much as those of the three DCPs do. Binding with CdSe NCs significantly alters the interactions among PS blocks. The ligand–cluster coordination is much stronger than other non-covalent interactions existed in the HDCPs, such as π–π stacking and alkyl chain interdigitation. It is thus reasonable to assume that it is the NC-binded PS block dictates solid state aggregation for all three hybrid DCPs, regardless of their initial PS block sizes, making all three hybrid DCPs with comparable solid state optical properties.

The HOMO/LUMO energy levels of the CdSe NCs, DCPs and HDCPs were studied by cyclovoltammetry (CV) measurements. Films of the TOPO/HDA-capped CdSe NCs, DCPs and HDCPs were prepared by drop-casting their solutions onto a Pt-disc working electrode. After drying under the flow of Argon, the CV measurements of all samples were run under identical conditions. As shown in Fig. 8, the cyclic voltammogram of pure CdSe NCs shows a clear reversible reduction wave with a half cell potential of −1.13 eV (*vs.* Fc/Fc^{+}), from which the LUMO energy level of CdSe NCs can be estimated to be ~−3.67 eV.

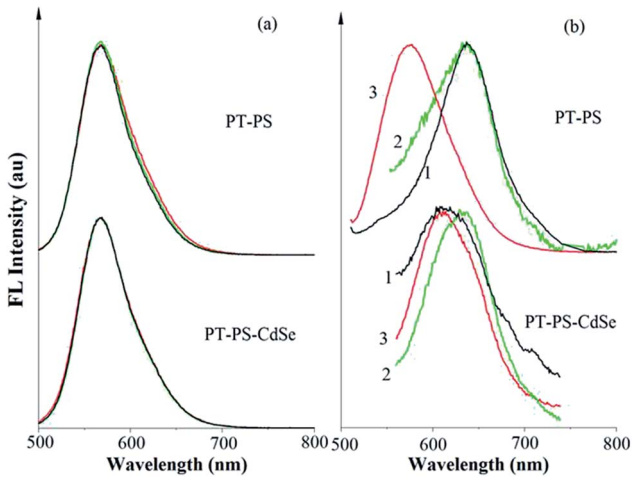

Fig. 7 Photoluminescence emission spectra of DCPs before and after CdSe coordination in dilution solutions (a) or as thin solid films (b).

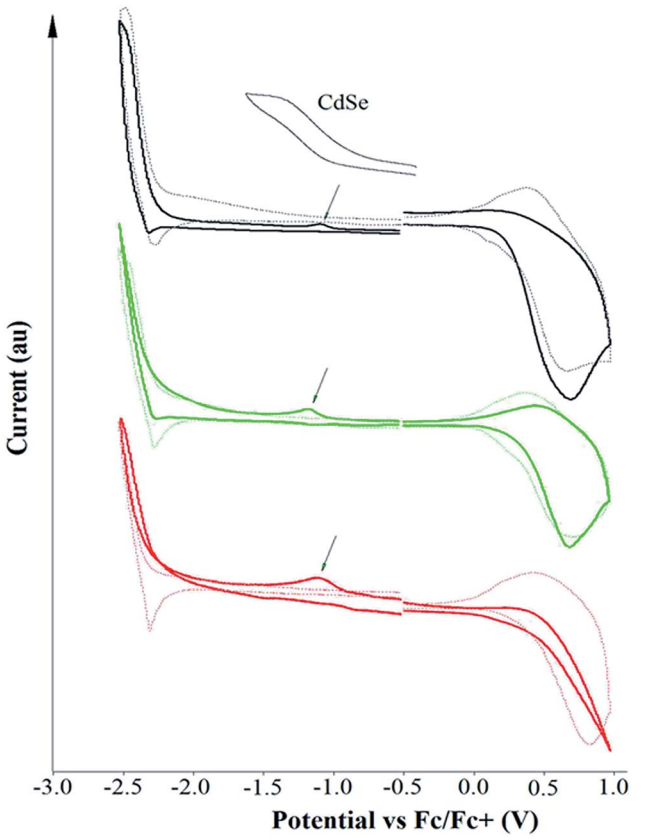

Fig. 8 Cyclic voltammograms of P3HT-PS-1 (black), P3HT-PS-2 (green) and P3HT-PS-3 (red) before (dotted line) and after (solid line) CdSe coordination.

There is no oxidation wave observed during the anodic scan. All DCPs and HDCPs show a similar reduction wave onsetting around −2.3 eV and a semireversible oxidation wave onsetting at 0.3 eV (*vs.* Fc/Fc^{+}), both of which are attributed to the P3HT block. Careful comparison shows that redox processes in HDCPs are all less reversible than those in DCPs. At a lower negative potential, all three HDCPs show a small but clear reduction hump with a peak potential around −1.1 eV. This hump is missing in the voltammograms of the three DCPs and can thus be attributed to the CdSe NCs. The observation of the reduction process of CdSe NCs in the HDCPs not only confirms the successful incorporation of the NCs in the HDCPs, but also indicates that those incorporated NCs are susceptible to electron transfers. Based on the redox onset potentials, one can calculate the HOMO and LUMO levels of the P3HT block to be −5.10 eV and −2.51 eV, respectively. The driving forces for potential charge transfer between the P3HT moiety and the CdSe NCs can be estimated by the Rehm–Weller equation,[46]

$$\Delta G = e[E_{ox}(D) - E_{red}(A)] - E_g - C \quad (1)$$

where ΔG is the free energy change (in eV) associated with the photoinduced charge transfer process, $E_{ox}(D)$ and $E_{red}(A)$ are the oxidation potential of the donor (P3HT) and the reduction potential of the acceptor (CdSe NCs), respectively, E_g is the bandgap of the donor or acceptor, and C is the Coulomb term which is *ca.* 0.06 eV in acetonitrile.[46] The free energy change associated with the electron transfer process from the excited P3HT moiety to the LUMO of the CdSe NCs is calculated to be −1.22 eV, while the free energy change associated with the hole transfer process from the excited CdSe NCs to the HOMO of the P3HT moiety is calculated to be −0.72 eV. The large negative free energy changes indicate that the charge transfer at the P3HT/CdSe NC interface is thermodynamically feasible.

To evaluate the photovoltaic properties of the HDCPs, regular photovoltaic cells with the configuration of glass/ITO/PEDOT:PSS/**P3HT-PS-CdSe**/Ca/Al as illustrated in Fig. 9a were fabricated. In general, the solar cells were fabricated by spin-coating the HDCP solutions on top of ITO/PEDOT:PSS, followed by the deposition of Ca/Al electrodes. Fig. 9b shows the *J–V* curves of the solar cells of **P3HT-PS-2** and **P3HT-PS-CdSe-2**, while Table 1 summarizes their *J–V* characteristics, including open circuit voltage (V_{OC}), short circuit current density (J_{SC}), fill factor (FF), and power conversion efficiency (PCE).

With film thickness of 80 ± 5, 140 ± 5 and 110 ± 5 nm, respectively, **P3HT-PS-CdSe-1–3** show rather high V_{OC}s but low J_{SC}s and poor fill factors. Estimated from the illuminated *J–V* curves, the series resistance of these solar cells is 1.35 kΩ cm^{-2} or greater which is large and likely contributed to the poor FF. Devices fabricated from **P3HT-PS-CdSe-2** give the highest PCE of 0.17%. Devices fabricated from the corresponding P3HT-PS DCPs (without CdSe attachment) gave PCEs of 0.01%, indicating that the attached CdSe NCs do help improving the device performance. The IPCE spectra of the devices, shown in Fig. 10b, reasonably match the absorption spectra of the corresponding thin films (Fig. 10a) especially in the visible range, confirming the photosensitivity contribution of the DCPs. There

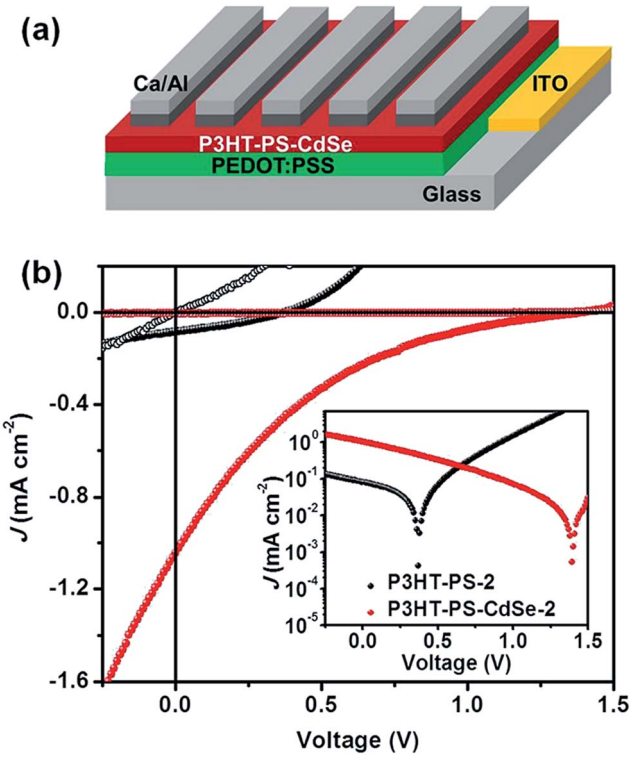

Fig. 9 (a) Device architecture. (b) Current density–voltage (*J–V*) curves (empty: dark; filled: illuminated) of the solar cells of glass/ITO/PEDOT:PSS/**P3HT-PS-2** or **P3HT-PS-CdSe-2**/Ca/Al. The illuminated curves were measured under AM 1.5 G 1-sun (100 mW cm^{-2}) illumination. For clear identification of V_{OC}s, the inset in (b) shows the illuminated *J–V* curves of the devices with the *J*-axis plotted in log-scale.

Table 1 Parameters of the photovoltaic cells under AM 1.5 G 1 Sun (100 mW cm^{-2}) illumination

Active material	V_{OC} (V)	J_{SC} (mA cm^{-2})	FF	PCE (%)
P3HT-PS-CdSe-1	1.40	0.217	0.125	0.038
P3HT-PS-CdSe-2	1.39	1.042	0.118	0.170
P3HT-PS-CdSe-3	1.13	0.119	0.158	0.021
P3HT-PS-2	0.37	0.083	0.324	0.010
P3HT : CdSe (1 : 8)	0.73	2.27	0.229	0.379

is a slight mismatch in the UV region between the IPCE spectra and the film absorption spectra, presumably due to the fact that the insulating PS block absorbs in the UV region as well (Fig. 10a inset) but produces no photocurrent. Only absorptions from CdSe and P3HT are expected to generate photocurrent. Although the coordinatively binded CdSe nanocrystals help improve the solar cell performance, the performance of these HDCPs is clearly not on par with those of the best P3HT:CdSe composites. There are a number of reasons for the HDCP's not so appealing performance. First of all, the incorporated CdSe NCs in the HDCPs is rather low. Among the three HDCPs, **P3HT-PS-CdSe-2** has the highest CdSe loading, which may be the reason why it showed the best performance. However, its NC loading is still only 40%. For P3HT:CdSe blends, the best

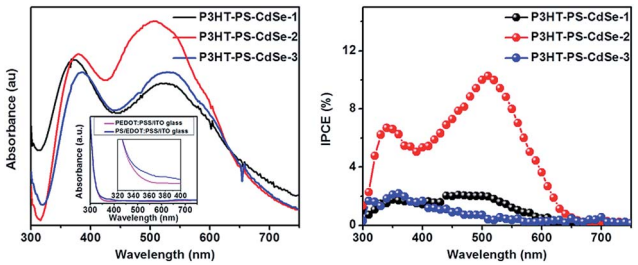

Fig. 10 (a) Absorption spectra of thermally annealed (at 120 °C for 10 min under nitrogen atmosphere) HDCP thin films fabricated on PEDOT:PSS/ITO substrates. The inset in (a) shows the absorption of the reference film of PEDOT:PSS/ITO glass (magenta) and the one with a very thin PS layer coated on it (royal). (b) IPCE spectra of the solar cells of glass/ITO/PEDOT:PSS/**P3HT-PS-CdSe**/Ca/Al.

performing devices typically have a P3HT to CdSe weight ratio around 1 : 8.[47] In other words, the weight percentage of CdSe in the blends is over 85%. The low NC content likely prevented the aggregation of NCs to form continuous electron transporting networks, which is supported by the TEM studies where NCs are shown to be isolated. The lack of morphologies supporting bicontinuous charge transporting pathways may also account for the poor fill factors. Another reason for the poor performance may be due to the short P3HT block length.[6] The P3HT in the HDCPs has an average molecular weight of only about 2300 while the best performing P3HT:CdSe blends has P3HTs with molecular weights over 100 000.[5] Regioregular P3HT with large molecular weight can self-organize and align polymer chains to form semicrystalline lamellar morphologies which possess highly ordered packing and alignment, high hole mobility, and strong interchain and interlayer interactions.[12] However, for all the three HDCPs in the present work, no long range order of P3HT packing was observed from their HRTEM images (Fig. 4). Indeed, a bulk heterojunction device using the short P3HT in the P3HT : CdSe (1 : 8) blends showed a PCE of only 0.38%, significantly lower than similar BHJ devices fabricated from high molecular weight P3HT : CdSe blends.[47] The fact that the **P3HT-PS-CdSe-2**, albeit with much lower CdSe loading, showed PCEs not that much lower than that of the corresponding P3HT : CdSe blend indicates again that coordination of NCs with the DCP backbone improves device performance. To increase CdSe NC loading in the HDCPs, PS blocks with higher density of binding ligands may be needed. Using a P3HT block with high enough molecular weights and a PS block with higher binding capacity to NCs, the resulting HDCPs are expected to show better performance.

4 Conclusions

In conclusion, three P3HT-PS rod coil DCPs containing phosphate or phosphine oxide binding ligands in the coil block have been synthesized. The three DCPs have the same P3HT block length but different sized coil blocks. While the three DCPs show nearly identical solution optical properties, the optical properties of their films with fluorescence wavelengths in particular differ significantly, reflecting different extent of interchain P3HT stacking in the solid state due to the different size disparity of the rod and coil blocks in the three DCPs. Binding with CdSe nanocrystals was achieved by ligand-exchange and was confirmed by FT-IR, TEM, EDX and TGA measurements. The resulting HDCPs showed very different optical properties from their corresponding DCPs, particularly in the solid state. The energy levels of HDCPs were studied by CV measurements and shown to be suitably aligned for PV devices. The HDCPs showed improved solar cell performance over their corresponding DCPs, confirming that the coordinatively binded CdSe nanocrystals help improve the initial photoinduced charge separation. The CdSe loading in the HDCPs is however very limited, presumably due to the low density of binding ligands in the coil block. As a result, the CdSe nanocrystals in the HDCPs are mostly isolated and not forming connected networks, which led to poor fill factors and lower than expected device efficiencies. The short P3HT block length also limited the device performance. Nevertheless, the beneficial effect of CdSe coordination is clearly demonstrated. When longer P3HT block is used and higher CdSe loading is achieved, significant improvement in solar cell performance is expected. The higher CdSe loading may be realized by increasing the density of binding ligands in the coil block or directly attaching binding ligands as side chain pendants to the P3HT rod block. Efforts along these lines are in progress.

Notes and references

1 C. J. Brabec, N. S. Sariciftci and J. C. Hummelen, *Adv. Funct. Mater.*, 2001, **11**, 15.
2 K. M. Coakley and M. D. McGehee, *Chem. Mater.*, 2004, **16**, 4533.
3 S. Günes, H. Neugebauer and N. S. Sariciftci, *Chem. Rev.*, 2007, **107**, 1324.
4 B. C. Thompson and J. M. J. Fréchet, *Angew. Chem., Int. Ed.*, 2007, **47**, 58.
5 M. Wright and A. Uddin, *Sol. Energy Mater. Sol. Cells*, 2012, **107**, 87.
6 P. Schilinsky, U. Asawapirom, U. Scherf, M. Biele and C. J. Brabec, *Chem. Mater.*, 2005, **17**, 2175.
7 H.-Y. Chen, J. Hou, S. Zhang, Y. Liang, G. Yang, Y. Yang, L. Yu, Y. Wu and G. Li, *Nat. Photonics*, 2009, **3**, 649.
8 Y. Liang, Z. Xu, J. Xia, S.-T. Tsai, Y. Wu, G. Li, C. Ray and L. Yu, *Adv. Mater.*, 2010, **22**, E135.
9 W. U. Huynh, J. J. Dittmer and A. P. Alivisatos, *Science*, 2002, **295**, 2425.
10 L. E. Greene, M. Law, B. D. Yuhas and P. Yang, *J. Phys. Chem. C*, 2007, **111**, 18451.
11 C. Y. Kuo, W. C. Tang, C. Gau, T. F. Guo and D. Z. Jeng, *Appl. Phys. Lett.*, 2008, **93**, 033307.
12 Y. Li, P. Lu, M. Jiang, R. Dhakal, P. Thapaliya, Z. Peng, B. Jha and X. Yan, *J. Phys. Chem. C*, 2012, **116**, 25248.
13 H.-J. Syu, S.-C. Shiu and C. F. Lin, *Sol. Energy Mater. Sol. Cells*, 2012, **98**, 267.
14 C.-Y. Liu, Z. C. Holman and U. R. Kortshagen, *Nano Lett.*, 2009, **9**, 449.

15 L. Wang, Y. Liu, X. Jiang, D. Qin and Y. Cao, *J. Phys. Chem. C*, 2007, **111**, 9538.
16 S. Ren, L.-Y. Chang, S.-K. Lim, J. Zhao, M. Smith, N. Zhao, V. Bulović, M. Bawendi and S. Gradečak, *Nano Lett.*, 2011, **11**, 3998.
17 W. U. Huynh, X. Peng and A. P. Alivisatos, *Adv. Mater.*, 1999, **11**, 923.
18 J. Yang, A. Tang, R. Zhou and J. Xue, *Sol. Energy Mater. Sol. Cells*, 2011, **95**, 476.
19 S. Kumar and T. Nann, *J. Mater. Res.*, 2004, **19**, 1990.
20 Y. Kang, N.-G. Park and D. Kim, *Appl. Phys. Lett.*, 2005, **86**, 113101.
21 J.-J. Wang, Y.-Q. Wang, F.-F. Cao, Y.-G. Guo and L.-J. Wan, *J. Am. Chem. Soc.*, 2010, **132**, 12218.
22 S. Günes, K. P. Fritz, H. Neugebauer, N. S. Sariciftci, S. Kumar and G. D. Scholes, *Sol. Energy Mater. Sol. Cells*, 2007, **91**, 420.
23 G. K. Mor, S. Kim, M. Paulose, O. K. Varghese, K. Shankar, J. Basham and C. A. Grimes, *Nano Lett.*, 2009, **9**, 4250.
24 Y.-Y. Lin, T.-H. Chu, S.-S. Li, C.-H. Chuang, C.-H. Chang, W.-F. Su, C.-P. Chang, M.-W. Chu and C.-W. Chen, *J. Am. Chem. Soc.*, 2009, **131**, 3644.
25 W. J. E. Beek, M. M. Wienk and R. A. J. Janssen, *Adv. Funct. Mater.*, 2006, **16**, 1112.
26 Y. Li, S. Li, L. Jin, J. B. Murowchick and Z. Peng, *RSC Adv.*, 2013, **3**, 16308.
27 R. Zhu, C. Y. Jiang, B. Liu and S. Ramakrishna, *Adv. Mater.*, 2009, **21**, 994.
28 L. Zhao and Z. Lin, *Adv. Mater.*, 2012, **24**, 4353.
29 X. Yang, J. Loos, S. C. Veenstra, W. J. H. Verhees, M. M. Wienk, J. M. Kroon, M. A. J. Michels and R. A. J. Janssen, *Nano Lett.*, 2005, **5**, 579.
30 J. Liu, T. Tanaka, K. Sivula, A. P. Alivisatos and J. M. J. Fréchet, *J. Am. Chem. Soc.*, 2004, **126**, 6550.
31 H. Skaff, K. Sill and T. Emrick, *J. Am. Chem. Soc.*, 2004, **126**, 11322.
32 L. Zhao, X. Pang, R. Adhikary, J. W. Petrich and Z. Lin, *Angew. Chem.*, 2011, **123**, 4044.
33 L. Zhao, X. Pang, R. Adhikary, J. W. Petrich, M. Jeffries-EL and Z. Lin, *Adv. Mater.*, 2011, **23**, 2844.
34 C. Y. Li, K. K. Tenneti, D. Zhang, H. Zhang, X. Wan, E. Chen, Q. Zhou, A. Carlos, S. Igos and B. S. Hsiao, *Macromolecules*, 2004, **37**, 2854.
35 C. L. Chochos, P. K. Tsolakis, V. G. Gregoriou and J. K. Kallitsis, *Macromolecules*, 2004, **37**, 2502.
36 Y. Tu, X. Wan, H. Zhang, X. Fan, X. Chen, Q. Zhou and K. Chau, *Macromolecules*, 2003, **36**, 6565.
37 R. Gref, P. Couvreur, G. Barratt and M. Evgueni, *Biomaterials*, 2003, **24**, 4529.
38 Z. Li, R. Jin, C. A. Mirkin and R. L. Letsinger, *Nucleic Acids Res.*, 2002, **30**, 1558.
39 S. P. Dudek, H. D. Sikes and C. E. D. Chidsey, *J. Am. Chem. Soc.*, 2001, **123**, 8033.
40 M. C. Iovu, M. Jeffries-El, E. E. Sheina, J. R. Cooper and R. D. McCullough, *Polymer*, 2005, **46**, 8582.
41 S. Chakraborty, J. Lu, Y. Li, Y. Liu, T. Dutta, D.-M. Zhu, X. Yan, A. Keightley and Z. Peng, *Eur. J. Inorg. Chem.*, 2013, **2013**, 1799.
42 D. Markova, A. Kumar, M. Klapper and K. Müllen, *Polymer*, 2009, **50**, 3411.
43 R. C. Shallcross, G. D. D'Ambruoso, B. D. Korth, H. K. Hall Jr, Z. Zheng, J. Pyun and N. R. Armstrong, *J. Am. Chem. Soc.*, 2007, **129**, 11310.
44 J. B. Katari, V. L. Colvin and A. P. Alivisatos, *J. Phys. Chem.*, 1994, **98**, 4109.
45 C. de Mello Donega, S. G. Hickey, S. F. Wuister, D. Vanmaekelbergh and A. Meijerink, *J. Phys. Chem. B*, 2003, **107**, 489.
46 Y. Li, L. Jin, S. Chakraborty, S. Li, P. Lu, D.-M. Zhu, X. Yan and Z. Peng, *J. Polym. Sci., Part B: Polym. Phys.*, 2014, **52**, 122.
47 M. J. Greaney, S. Das, D. H. Webber, S. E. Bradforth and R. L. Brutchey, *ACS Nano*, 2012, **6**, 4222.